Short Article

Cell Metabolism

Elevated Levels of the Reactive Metabolite Methylglyoxal Recapitulate Progression of Type 2 Diabetes

Graphical Abstract

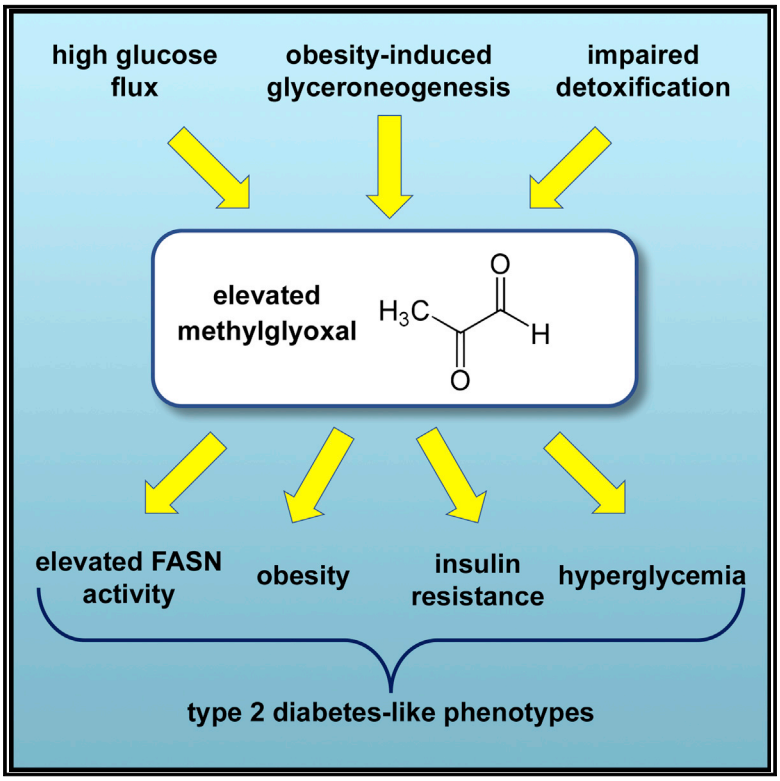

Highlights

- Elevated levels of methylglyoxal (MG) induce obesity and hyperglycemia in *Drosophila*
- Flies with elevated MG have high fatty acid synthase (FASN) activity
- MG forms adducts on FASN
- Elevated MG causes insulin resistance in *Drosophila*

Authors

Alexandra Moraru, Janica Wiederstein, Daniel Pfaff, Thomas Fleming, Aubry K. Miller, Peter Nawroth, Aurelio A. Teleman

Correspondence

a.teleman@dkfz.de

In Brief

Moraru et al. find that elevated levels of the reactive metabolite methylglyoxal in a *Drosophila* model recapitulate the progression of type 2 diabetes, causing flies to become obese, insulin resistant, and hyperglycemic. This raises the question of whether elevated methylglyoxal might be a cause of type 2 diabetes.

Moraru et al., 2018, Cell Metabolism *27*, 1–9
April 3, 2018
https://doi.org/10.1016/j.cmet.2018.02.003

CellPress

Please cite this article in press as: Moraru et al., Elevated Levels of the Reactive Metabolite Methylglyoxal Recapitulate Progression of Type 2 Diabetes, Cell Metabolism (2018), https://doi.org/10.1016/j.cmet.2018.02.003

Cell Metabolism
Short Article

Elevated Levels of the Reactive Metabolite Methylglyoxal Recapitulate Progression of Type 2 Diabetes

Alexandra Moraru,[1,2] Janica Wiederstein,[1,2,6,7] Daniel Pfaff,[1,2,3,4,5,7] Thomas Fleming,[3,4,5] Aubry K. Miller,[1] Peter Nawroth,[3,4,5] and Aurelio A. Teleman[1,2,8,*]
[1]German Cancer Research Center (DKFZ), 69120 Heidelberg, Germany
[2]Heidelberg University, 69120 Heidelberg, Germany
[3]Department of Internal Medicine I and Clinical Chemistry, Heidelberg University Hospital, 69120 Heidelberg, Germany
[4]German Center for Diabetes Research (DZD), 85764 Neuherberg, Germany
[5]Joint Heidelberg-IDC Translational Diabetes Program, Helmholtz-Zentrum, 85764 Munich, Germany
[6]Present address: Institute for Genetics, Cologne Excellence Cluster on Cellular Stress Responses in Aging-Associated Diseases (CECAD), 50931 Cologne, Germany
[7]These authors contributed equally
[8]Lead Contact
*Correspondence: a.teleman@dkfz.de
https://doi.org/10.1016/j.cmet.2018.02.003

SUMMARY

The molecular causes of type 2 diabetes (T2D) are not well understood. Both type 1 diabetes (T1D) and T2D are characterized by impaired insulin signaling and hyperglycemia. From analogy to T1D, insulin resistance and hyperglycemia are thought to also play causal roles in T2D. Recent clinical studies, however, found that T2D patients treated to maintain glycemia below the diabetes definition threshold (HbA_{1c} < 6.5%) still develop diabetic complications. This suggests additional insulin- and glucose-independent mechanisms could be involved in T2D progression and/or initiation. T2D patients have elevated levels of the metabolite methylglyoxal (MG). We show here, using *Drosophila* glyoxalase 1 knockouts, that animals with elevated methylglyoxal recapitulate several core aspects of T2D: insulin resistance, obesity, and hyperglycemia. Thus elevated MG could constitute one root cause of T2D, suggesting that the molecular causes of elevated MG warrant further study.

INTRODUCTION

Type 2 diabetes (T2D) is a leading cause of morbidity and mortality in western nations. The molecular causes of T2D are not well understood, making it difficult to develop a targeted therapy. Although multiple different clinical aspects have been associated with this disease, at its core T2D is characterized by a combination of insulin resistance, hyperglycemia, and obesity (Han and Lean, 2016). In analogy to T1D, in which impaired insulin signaling due to autoimmune destruction of pancreatic β cells is the cause of the disease, insulin resistance and hyperglycemia have been thought to play causal roles in T2D development as well. Indeed, elevated circulating glucose, reflected by elevated glycation of hemoglobin (HbA_{1c}), correlates with incidence of diabetic complications. Several studies have shown that for diabetic patients with HbA_{1c} above 7.5%, a drop in HbA_{1c} of 1% leads to a 10%–15% drop in the risk of stroke or myocardial infarction and a 25% drop in microvasculature complications (Yudkin et al., 2010). This holds true, however, only down to an HbA_{1c} of 7.5%. More recently, the ACCORD, ADVANCE, and VADT studies showed that intensive glycemic control aimed at bringing HbA_{1c} below 7.5% had no, or even detrimental, effects compared with standard therapy (Brown et al., 2010). Indeed, the ACCORD study had to be terminated prematurely due to increased mortality in the intensive therapy group, which aimed to bring the patients to an HbA1c below the diabetes definition threshold (Ismail-Beigi et al., 2010). Hence, there is a U-shaped relationship between HbA_{1c} levels and incidence of complications, with a minimum risk at roughly 7.5% HbA_{1c}. In agreement with this, overall survival of T2D patients also has a U-shaped relationship relative to HbA_{1c} with a minimal hazard ratio at HbA_{1c} of 7.5% (Currie et al., 2010). Importantly, however, diabetic patients with an HbA_{1c} of 7.5% still develop complications such as polyneuropathy, which non-diabetics do not develop. The ACCORD study found that patients with either standard glycemic control with an HbA_{1c} of 7.6% or intensive glycemic control with an HbA_{1c} of 6.3% still developed microalbuminuria, with a 12%–15% incidence rate during the 7 years of the study, and 45%–47% of the patients developed neuropathy (Ismail-Beigi et al., 2010), both of which are significantly higher than the incidence rate in non-diabetics. In sum, in type 2 diabetic patients with optimal glycemic control, the disease still progresses. This raises the possibility that additional underlying mechanisms independent of insulin and glucose may be responsible for disease progression, and possibly also for disease initiation. In fact, the ADDITION study identified a subset of people with high risk for developing T2D that have normal glucose tolerance (Skriver et al., 2010). Together, these studies raise the possibility that insulin resistance and hyperglycemia

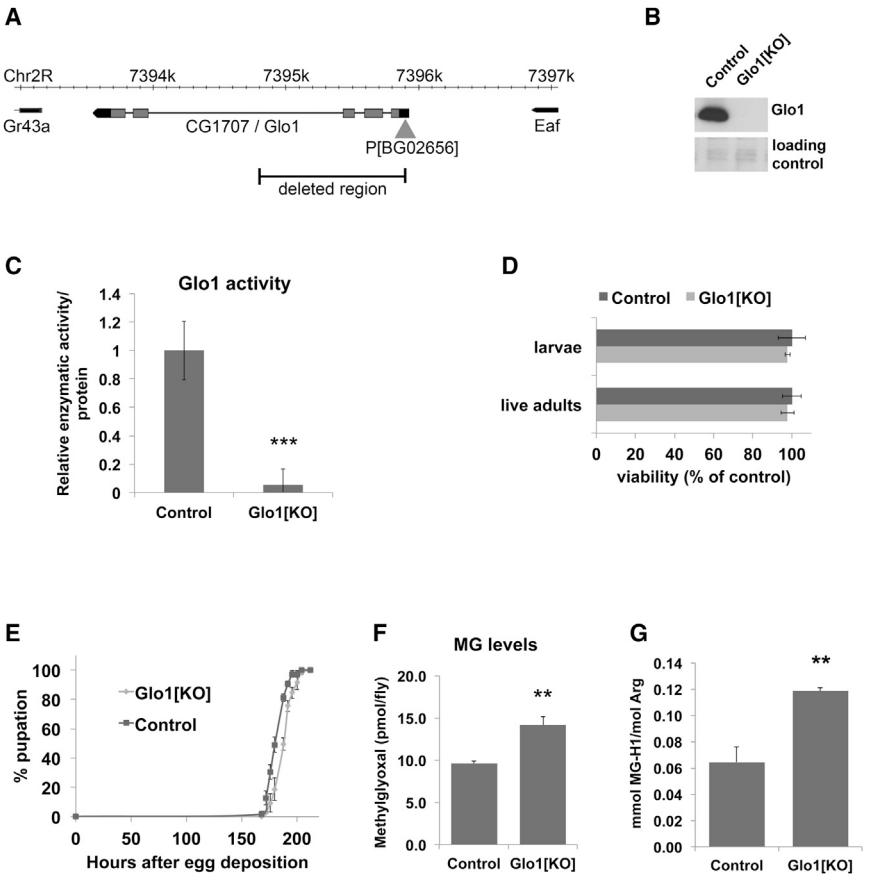

Figure 1. Glo1 Knockout *Drosophila* Have Elevated MG but Are Viable

(A) Map of the Glo1 (CG1707) genomic locus, indicating the deleted region of 1,136 nt containing the translation start site of the Glo1 gene. Glo1 5′ UTR and 3′ UTR indicated in black, open reading frame in gray, and introns as lines.

(B and C) Glo1^{KO} homozygous flies completely lack any detectable Glo1 protein detected by immunoblotting (B, male adults) or glyoxalase enzymatic activity (C, n = 10 male adults).

(D and E) Glo1^{KO} homozygous flies are viable (D) and have normal developmental timing (E). (D) Percentage live larvae ("larvae") hatching from 3 × 100 embryos, and percentage live adults ("adults") eclosing from 4 × 50 first-instar larvae are indicated. (E) Developmental timing shown as time from egg deposition to pupation (n = 4 × 50).

(F) Free methylglyoxal levels are elevated in Glo1^{KO} flies (n = 3 × 25 adult females).

(G) MG-H1 levels are elevated in Glo1^{KO} flies. MG-H1 levels quantified by mass spectrometry on fully hydrolyzed whole-fly lysates, normalized to arginine levels (n = 3 × 10 adult females).

Error bars: SD. **p < 0.01, ***p < 0.001; t test.

might be epiphenomena: symptoms that result from the disease, but are not part of the causal cascade leading to T2D. If this is the case, an important open issue is the identification of the molecular causes of T2D.

Methylglyoxal (MG) is a reactive metabolite that forms as a by-product of flux through various metabolic pathways, including glycolysis (Rabbani and Thornalley, 2015; Ramasamy et al., 2006; Thornalley and Rabbani, 2011). MG reacts directly with lysine and arginine residues on proteins to form advanced glycation end products that affect protein function (Thornalley, 2008). Exogenous administration of MG, either orally to mice and rats or to cells in culture, results in physiological changes observed in diabetic patients such as collagen accumulation in kidneys, hypercholesterolemia, microvasculature degeneration, and insulin resistance (Berlanga et al., 2005; Golej et al., 1998; Riboulet-Chavey et al., 2006). The physiological relevance of these models, however, is unclear, since they rely on high exogenous MG applied from the outside of cells, rather than elevated levels of intracellular, endogenous MG. One mechanism known to detoxify MG is the glyoxalase system, composed of two enzymes, glyoxalase 1 (Glo1) and glyoxalase 2, which act sequentially to convert MG into D-lactate (Rabbani and Thornalley, 2015; Ramasamy et al., 2006; Thornalley, 2008; Thornalley and Rabbani, 2011). Partial reduction of Glo1 function in mice leads to hyperalgesia, also observed in diabetic patients (Bierhaus et al., 2012), as well as nephropathy similar to diabetic nephropathy (Giacco et al., 2014), suggesting that these two phenotypes are particularly sensitive to mild impairments in Glo1 activity. Until now, however, no Glo1 complete loss-of-function vertebrate animals have been reported. While our manuscript was in revision, Glo1 knockout worms were reported, which have an astounding 3,000-fold elevation in MG and develop hyperesthesia and neuronal damage (Chaudhuri et al., 2016).

Drosophila has emerged as a useful model system to study human diseases including neurodegenerative disease, cancer, and metabolic dysfunction (Bellen and Yamamoto, 2015). We study here the consequences of elevated endogenous MG by generating and characterizing Glo1 knockout *Drosophila*. Surprisingly, we find that impaired MG detoxification causes the animals to progressively develop the core characteristics of T2D: insulin resistance, obesity, and hyperglycemia. Since elevated MG can recapitulate T2D phenotypes, this raises the possibility that elevated MG could constitute one cause of the disease.

RESULTS

Glo1 Knockout Animals Have Elevated MG but Are Viable

To study the consequences of elevated MG levels *in vivo*, we generated Glo1 loss-of-function flies, lacking the translation start site and much of the open reading frame (Figure 1A), leading to flies with no Glo1 protein (Figure 1B) and no detectable Glo1 activity above background (Figure 1C). We refer to these animals as Glo1^{KO}. Unexpectedly, Glo1^{KO} are viable (Figure 1D) and have no defects in patterning, size, or developmental rate (Figures 1E and S1A), but as expected have elevated levels of free MG (Figure 1F). Levels of MG-H1, an adduct formed by MG on arginines of proteins, are also correspondingly elevated (Figure 1G). Since

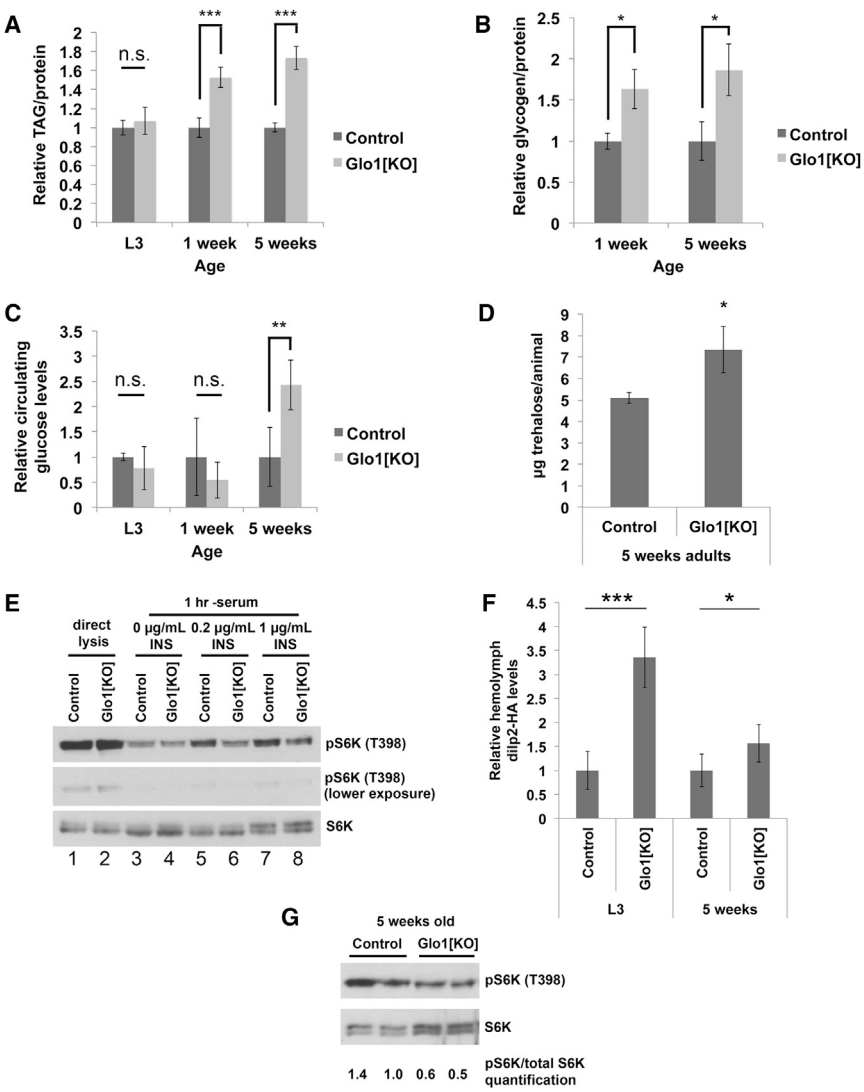

Figure 2. Glo1 Mutant Animals Progressively Develop Diabetes-like Phenotypes with Age

(A) Glo1^{KO} animals progressively become obese as they age. Total body triglyceride levels normalized to total body protein are indicated. L3, third-instar larvae. 1 or 5 weeks of age = adults (n = 4 × 8 females for L3 and 1 week time points, n = 3 × 8 for 5 weeks time point).

(B) Glo1^{KO} adults have elevated total body glycogen levels, normalized to total body protein (n = 3 × 8 females).

(C) Glo1^{KO} animals become hyperglycemic with older age. Circulating hemolymph glucose levels are shown (n = 4 × 10 females for L3 animals, n = 4 × 40 females at 1 and 5 weeks).

(D) Glo1^{KO} animals have elevated circulating trehalose levels at 5 weeks of age (n = 3 × 6 females).

(E) Glo1^{KO} animals display insulin resistance starting early in development. Control or Glo1^{KO} third-instar female larvae were either lysed directly or first explanted into Schneider's medium lacking serum for 1 hr and then stimulated for 15 min with increasing amounts of insulin as indicated. Activation of the insulin/PI3K/TORC1 pathway was detected via phosphorylation of the canonical TORC1 target S6K (n = 6 animals per sample). INS, insulin.

(F) Glo1^{KO} animals have strongly elevated circulating insulin levels relative to controls early in development and mildly elevated levels at 5 weeks of adult age. ELISA on dILP2-HA from hemolymph of control or Glo1^{KO} third-instar larvae (n = 7 × 7 larvae) or 5-week-old adults (5 × 30 flies).

(G) Glo1^{KO} adults have reduced phosphorylation of S6K at the insulin-sensitive site at 5 weeks of age (n = 2 × 6 animals).

Error bars: SD. *p < 0.05, **p < 0.01, ***p < 0.001; t test.

viability of these animals was somewhat unexpected, we tested for compensatory changes in the expression of genes involved in the oxidative stress response (Nrf2 targets), in glucose sensing and uptake (Mondo/Mlx targets; Sykiotis and Bohmann, 2008; TXNIP), or genes known to compensate for Glo1 loss of function in cell culture models (e.g., AKR; Morgenstern et al., 2017) (Figure S1B). Expression of none of these genes was upregulated, except for the TXNIP homolog CG2993. We also did not find an upregulation in aldo-keto reductase enzymatic activity (Figures S1C and S1D′), which was previously found to be elevated in Glo1 knockout mouse Schwann cells (Morgenstern et al., 2017), nor could we detect any MG dehydrogenase activity above background in fly lysates (Figures S1E and S1E′). However, since MG levels are ~50% elevated in Glo1^{KO} flies, the total rate of MG reduction via this enzyme is also ~50% higher in the Glo1^{KO} flies, which may contribute to its detoxification. Future work will be necessary to identify whether any compensatory changes allow Glo1^{KO} flies to be viable. Nonetheless, we found that Glo1^{KO} animals have metabolic phenotypes, as outlined below, which are the focus of this study.

Glo1 Knockout Animals Progressively Become Insulin Resistant, Obese, and Hyperglycemic

To analyze the phenotypes of Glo1^{KO} in more detail, we undertook a metabolic characterization of these animals. Glo1^{KO} animals have normal total body triglyceride (triacylglycerol [TAG]) levels during their juvenile stages (L3, third-instar larvae) (Figure 2A), but progressively become obese in adulthood (Figure 2A; 1 and 5 weeks of age). *Drosophila* store triglycerides in the fat body, which serves the combined functions of human liver and adipose tissue. As in humans, flies store energy as both TAG and glycogen, and the levels of these two often correlate. Consistent with this, Glo1^{KO} animals also have elevated glycogen stores (Figure 2B). These phenotypes are rescued by expressing Glo1 from a transgene in the Glo1^{KO} animals, confirming they are specific to the Glo1 mutation (Figures S1F and S1G). We then quantified levels of glucose in circulation (in hemolymph) and found they are not significantly different from controls in juvenile animals and in early adulthood (Figure 2C; L3 and 1 week). Glo1^{KO} animals become hyperglycemic, however, at 5 weeks of age, corresponding to mid-life in humans

(Figure 2C). Likewise, at 5 weeks of age, levels of another circulating sugar, trehalose, are also elevated (Figure 2D). Thus, early in life Glo1^{KO} animals maintain euglycemia but increase TAG and glycogen storage, but when middle aged they become additionally hyperglycemic, suggesting a progressive breakdown in their capability to maintain homeostasis, recapitulating the progression seen in T2D patients.

To analyze this at the molecular level, we measured insulin signaling in Glo1^{KO} animals, both during development and at middle age, using S6K and Akt phosphorylation as canonical readouts for activation of the insulin/PI3K/TORC1 pathway in *Drosophila*. Insulin signaling levels were not strongly affected in young Glo1^{KO} animals ("direct lysis" lanes 1 and 2 in Figures 2E and S2A; for pS6K, see short exposure). Importantly, insulin signaling levels reflect the combination of insulin levels and tissue insulin sensitivity. To specifically assay insulin sensitivity, we explanted tissues for 1 hr into Schneider's medium lacking serum. This causes pS6K and pAkt levels to drop due to removal of insulin (Figures 2E and S2A, lanes 3 and 4). Re-stimulation of the tissues with insulin at two different concentrations (0.2 and 1 μg/mL) revealed that Glo1^{KO} tissues are insulin resistant, displaying impaired induction of S6K phosphorylation in response to defined insulin concentrations in the medium (Figures 2E and S2A, lanes 5–8). Since these animals maintain normal insulin signaling (lanes 1 and 2) despite tissue insulin resistance (lanes 5–8), this suggests they likely compensate by elevating levels of circulating insulin (in *Drosophila* insulin-like peptides, dILPs). Indeed, an ELISA for circulating dILP2-HA revealed that Glo1^{KO} flies have 3-fold elevated levels of circulating insulin in juvenile stages compared with controls (Figure 2F). Consistent with a progressive breakdown in metabolic control, Glo1^{KO} animals no longer have as strongly elevated circulating insulin levels at 5 weeks of age as they did earlier (Figure 2F). This correlates with reduced total-body insulin signaling (Figure 2G) and with the occurrence of hyperglycemia at 5 weeks of age (Figure 2C). In sum, these data show that elevated levels of MG cause a progressive breakdown of metabolic control that worsens with age, reminiscent of what is seen in T2D patients. At early stages, Glo1^{KO} animals are insulin resistant, but compensate with elevated circulating insulin levels, causing their glycemia and adiposity to be normal. In early adulthood, Glo1^{KO} flies still maintain euglycemia but become obese. Later in life, this buffering mechanism also breaks down, leading to reduced total-body insulin signaling and hyperglycemia.

Glo1 Knockouts Have Elevated FASN Activity

One possible explanation for the elevated adiposity of Glo1^{KO} animals is impaired lipid mobilization. Glo1^{KO} animals, however, have a normal respiratory quotient (Figures S2B), suggesting normal levels of fatty acid β-oxidation. Furthermore, Glo1^{KO} animals mobilize lipids as efficiently as, if not more efficiently than, control animals when challenged with 12 hr of fasting (Figure S2C). This suggests Glo1^{KO} animals may instead have elevated fatty acid biosynthesis. Indeed, Glo1^{KO} animals have mildly elevated food intake (Figure S2D). We quantified fatty acid synthase (FASN) activity in 1-week-old adults and found it to be significantly elevated in Glo1^{KO} animals compared with controls (Figure 3A). This was not due to elevated levels of FASN1 protein in the lysates of Glo1^{KO} animals (Figure 3B) or elevated FASN1 expression (Figure S2E). Interestingly, a recent report also found interconnections between Glo1 and FASN (Garrido et al., 2015).

To test whether this is a cell-autonomous effect, we asked whether treatment of cells in culture with MG causes elevated FASN activity. We first sought to determine the concentration of MG that needs to be added to the culture medium. Addition of MG to culture medium causes extracellular and intracellular MG levels to transiently peak and then progressively return to baseline within 24 hr of treatment (Figure S3A) either due to MG detoxification by the cells or by reaction of the MG with proteins in the cells and in the medium. This transient kinetics makes it difficult to find a concentration that mimics elevated steady-state MG levels in an organism such as the Glo1 knockout fly. Instead, we used the minimum concentration of MG that induces elevated protein modification in the cells. To study protein modification by MG, we generated an antibody that detects the advanced glycation end product MG-H1, an MG adduct on arginine (Rabbani and Thornalley, 2015), by immunizing animals with MG-H1 conjugated to keyhole limpet hemocyanin (KLH). This yielded an antibody that specifically recognizes MG-H1-modified proteins by ELISA (Figure S3B) and gives a clear signal on immunoblots of lysates from cells treated with MG (Figure S3C). Using this antibody, we found that a single treatment of 1 mM MG was the minimum concentration that induced MG-H1 formation in *Drosophila* S2 cells (Figure S3D). A single treatment of *Drosophila* S2 cells with 1 mM MG led to depletion of FASN1 protein from the soluble fraction of cell lysates (Figure 3C), partly due to a drop in FASN1 expression (Figure S3E) and partly due to modified FASN1 protein pelleting into the insoluble fraction. Nonetheless, FASN activity in the soluble fraction is increased in lysates of cells treated with MG (Figure 3D), indicating that FASN1 protein from MG-treated cells is highly active compared with controls. One possibility is that FASN1 protein is directly modified by MG. We immunoprecipitated FASN1 from S2 cells treated once with 1 mM MG and found that, indeed, FASN1 becomes highly modified with MG-H1 adducts (Figure 3E). As an additional assay for direct modification of FASN1 by MG, we tested whether adding physiologically relevant levels of MG into cell lysates leads to elevated formation of MG-H1 adducts on FASN1, similar to what has previously been done for other proteins (Godfrey et al., 2014). We first treated S2 cell lysates with a titration of MG for 6 hr, and then quantified adduct levels by hydrolyzing the lysates completely to single amino acids and directly measuring MG-H1 levels by mass spectrometry (Figure S3F). This revealed that treating the lysates with 1 mM MG for 6 hr leads to a 2-fold increase in MG-H1 levels, which is significantly less than the 10-fold increase observed in diabetic patients (Ahmed et al., 2005). We then quantified MG-H1 levels on FASN1 immunoprecipitated from S2 cell lysates that had been treated with or without 0.5 mM MG, which causes MG-H1 levels to increase on average 30% proteome wide (Figure S3F). First, we observed that FASN1 is highly modified compared with the proteome on average, with circa 6 mmol of MG-H1 per mole of arginine, compared with 0.2 mmol MG-H1 per mole of arginine in untreated whole-cell lysates (Figures S3F and S3G). Thus, MG-H1 modifications can be readily detected by mass spectrometry on FASN1, and FASN1 is highly susceptible to such modifications compared

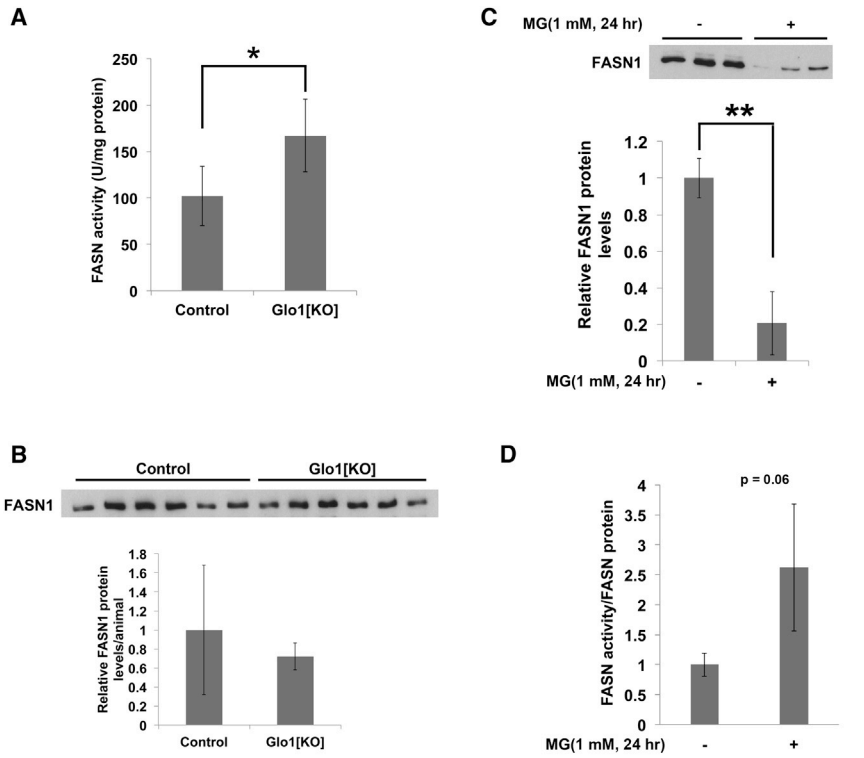

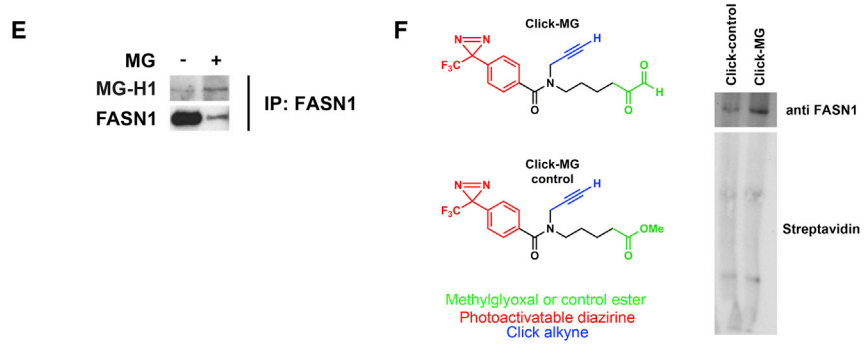

Figure 3. Elevated MG Leads to Increased FASN Modification and Activity

(A and B) Glo1^{KO} adults have elevated fatty acid synthase (FASN) activity (A) despite mildly reduced FASN protein levels in the lysates (B) (n = 5 × 6 females).

(C and D) FASN activity (D) is increased in cells treated with MG (1 mM, 24 hr) despite strongly reduced FASN1 protein levels in the same lysates (C) (n = 3 × ~5 million cells).

(E) FASN1 protein becomes strongly MG-H1 modified upon treatment of S2 cells with MG (3 mM, 24 hr). FASN1 was immunoprecipitated from S2 cells and blotted with MG-H1 antibody.

(F) FASN1 is modified by MG, detected via purification of proteins covalently attached to a "click" variant of MG and immunoblotting for FASN1. Left side: chemical structure of click-MG, containing the following functional groups: a bioreactive MG group (green), a photoactivatable diazirine cross-linker (red), and a bioorthogonal alkyne group (blue), which can be used to attach biotin to the compound *in vitro*. A compound in which the MG group is replaced with a methyl ester was used as a control. Right side: *Drosophila* S2 cells were treated with 10 μM click-MG or the control compound for 1 hr prior to cross-linking, addition of biotin, purification via streptavidin beads, and detection of FASN1 via immunoblotting.

Error bars: SD. *p < 0.05, **p < 0.01; t test.

with the average protein. Second, treatment of lysates with MG caused MG-H1 modification levels on FASN1 to increase significantly (Figure S3G).

Although upon extended exposure of proteins, MG forms irreversible adducts such as MG-H1, upon short-term exposure MG forms reversible adducts, such as hemithioacetals on cysteine residues (Thornalley, 1996). In fact, it is estimated that >90% of all MG in a cell is not free, but rather reversibly bound to cellular proteins (Thornalley, 1996). These adducts, however, are difficult to isolate biochemically because they are unstable. To circumvent this problem, we used an approach frequently employed to stabilize transient interactions such as ligand-receptor interactions or small molecule-protein interactions, whereby a photoactivatable diazirine cross-linker is added to the molecule of interest (Lenz et al., 2011). Upon photoactivation, the diazirine ring forms a reactive carbene, with a short half-life, causing the molecule of interest to be covalently attached to whichever protein is most proximal. We synthesized a derivative of MG, which we term "click-MG," with two additional functional groups: a diazirine ring and an alkyne group, which can be used after cell lysis to covalently attach the probe to biotin for purification via copper-catalyzed azide-alkyne cycloaddition ("click chemistry") (Figures 3F and S3H). We also synthesized an analogous control probe in which the glyoxal functional group was replaced with a methyl ester (Figure 3F). We treated *Drosophila* S2 cells with 10 μM click-MG or control probe for 60 min, then photoactivated the probe by exposing the cells to 365 nm light, then lysed the cells and covalently attached biotin, and finally purified the attached proteins via streptavidin beads (Figure S3H). Immunoblotting with FASN1 antibody revealed FASN1 is enriched in the click-MG precipitate compared with the control (Figure 3F), whereas on average other proteins are not (streptavidin blot; Figure 3F). This suggests MG might form reversible adducts on FASN1 at concentrations close to the ones found *in vivo*.

Methylglyoxal Alters Animal Physiology and Can Extend Lifespan

One source of MG is the spontaneous degradation of the glycolytic intermediates dihydroxyacetone phosphate (DHAP) and glyceraldehyde 3-phosphate (G3P). Hence, MG production is expected to increase if levels of DHAP and G3P rise as a consequence of an imbalance in production versus usage of DHAP and G3P, i.e., increased glucose uptake and flux through the first

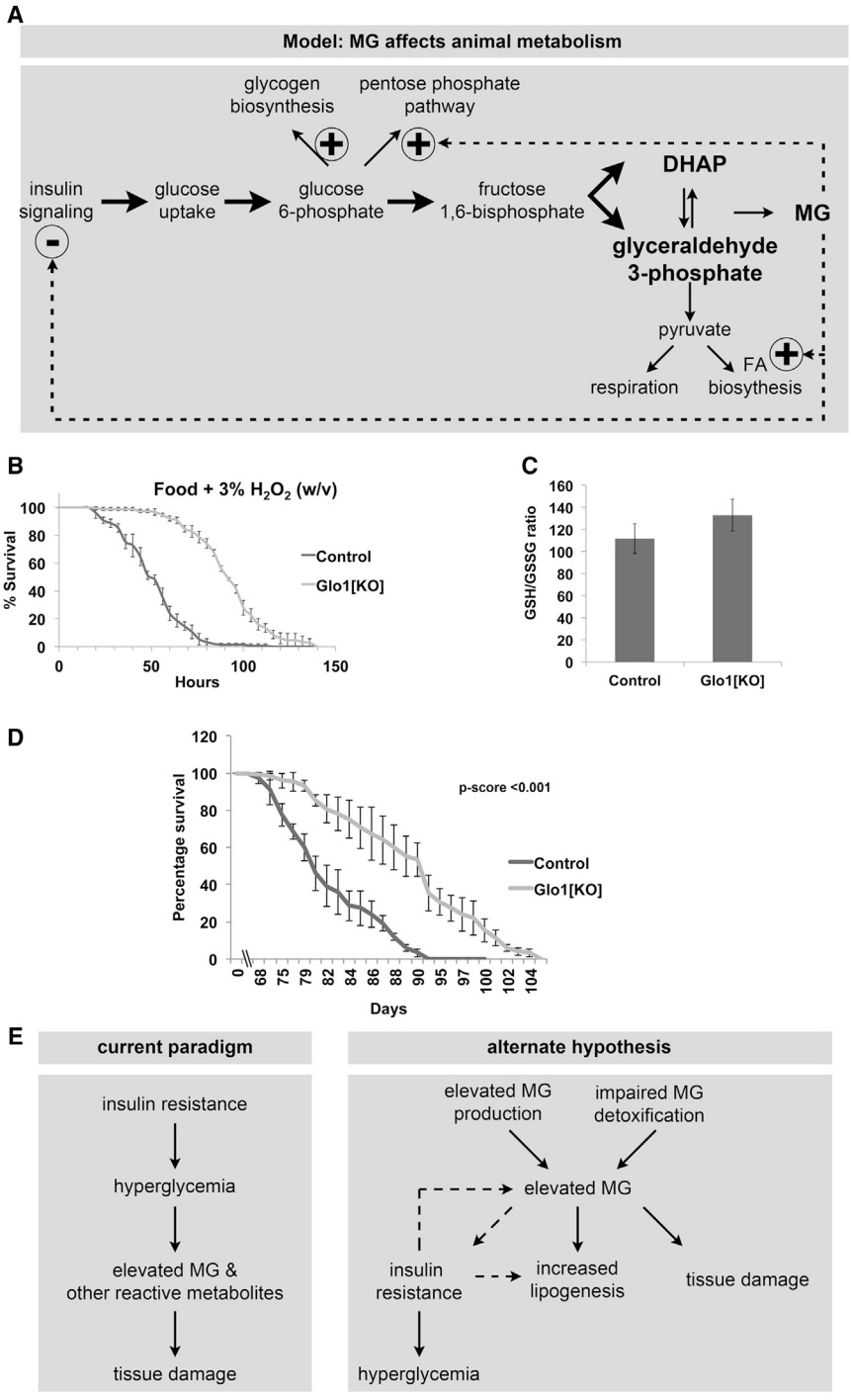

Figure 4. Methylglyoxal Affects Animal Metabolism

(A) Schematic diagram providing a rationalization of the effects observed upon increased MG *in vivo*. MG is generated during the interconversion of dihydroxyacetone phosphate (DHAP) and glyceraldehyde 3-phosphate. Elevated MG is expected to result when these intermediates accumulate due to elevated glucose uptake (bold arrows) and reduced usage (small arrows) of these intermediates. The data presented here are consistent with MG affecting animal metabolism and physiology by inhibiting glucose uptake and promoting alternate usage of intracellular glucose so as to renormalize DHAP and glyceraldehyde 3-phosphate levels. FA, fatty acid.

(B and C) $Glo1^{KO}$ flies have increased survival to oxidative stress (B, food supplemented with 3% H_2O_2 at 1 week of age) ($n = 3 \times 50$ females, $p < 0.001$ by log-rank significance test) and more reduced glutathione (C) ($n = 4 \times 10$ 1-week-old females, $p = 0.07$).

(D) $Glo1^{KO}$ flies have increased lifespans compared with control flies, consistent with reduced insulin signaling ($n = 3 \times 50$ females, $p < 0.001$ by log-rank significance test).

(E) Schematic diagram illustrating the current dominating paradigm that insulin resistance and hyperglycemia are root causes for T2D, and a new mechanistic explanation arising from this work, suggesting that elevated MG levels due to either elevated production or impaired detoxification may be a root cause of T2D.

Error bars: SD.

steps of glycolysis (thick arrows, Figure 4A) or reduced usage of pyruvate (thin arrow, Figure 4A). One way to rationalize the phenotypes described here is that MG can be considered a cellular proxy for unbalanced DHAP/G3P flux. MG feeds back on cellular metabolism to reduce production of DHAP and G3P by reducing insulin signaling and hence glucose uptake, and by increasing glycogen biosynthesis. Furthermore, MG increases usage of DHAP/G3P by increasing TAG biosynthesis (Figure 4A). This rationalization would predict that MG should also divert glucose flux into the pentose phosphate pathway, which provides NADPH both for lipid biosynthesis and to resist oxidative stress. To test this, we subjected $Glo1^{KO}$ animals to food supplemented with H_2O_2 (see Figures S4A and S4B for H_2O_2 titration) and found that they are significantly more resistant to oxidative stress compared with control animals (Figures 4B and S4D). A similar result was obtained if the H_2O_2 was simply added to a medium containing glucose and agar, indicating the phenotype is likely not due to the H_2O_2 reacting with components of the food to produce toxic metabolites (Figure S4C). The elevated resistance to oxidative stress is accompanied by an increase in the ratio of reduced-to-oxidized glutathione in $Glo1^{KO}$ animals (Figure 4C). Together with the fact that $Glo1^{KO}$ animals are viable, this rationalization would change the way we consider MG from being simply a toxic metabolite to a molecule that can affect animal metabolism and physiology. Indeed, we found that $Glo1^{KO}$ animals, which have elevated MG levels, have an extended lifespan compared with controls (Figure 4D). These data indicate that physiological MG can also have beneficial effects.

DISCUSSION

We find here that animals with elevated MG levels recapitulate several of the phenotypes associated with T2D. Pre-diabetic people have higher insulin levels than normal, which are needed by the body to maintain euglycemia. This is because their tissues are partially insulin resistant, as can be seen by elevated circulating glucose when challenged with an oral glucose tolerance test. This phase is often associated with weight gain. Over time, this constantly elevated insulin output cannot be maintained and for unknown reasons β cell exhaustion occurs, whereby circulating insulin levels are still elevated, but not elevated enough to compensate for the insulin resistance, leading to hyperglycemia. Similarly, we find that $Glo1^{KO}$ animals first become insulin resistant (Figure 2E). At this stage, $Glo1^{KO}$ animals compensate for the insulin resistance by elevating their circulating insulin levels to roughly 3.5 times the level of wild-type animals. Correspondingly, we do not detect reduced insulin signaling levels *in vivo* at these early stages or metabolic abnormalities. As the animals age, however, they first become obese, but not diabetic, observed as elevated total-body triglyceride with normal circulating glucose levels. At 5 weeks of age, which corresponds to circa 50 years of age in humans, circulating insulin levels in $Glo1^{KO}$ animals drop to 1.5 times the level of controls. At this point, although circulating insulin levels are still higher than controls, they are not high enough to compensate for the insulin resistance because the levels of insulin signaling drop below control levels (Figure 2G) and the animals become hyperglycemic (Figure 2C). At this stage of phenotypic progression, the increased lipid accumulation likely results from a combination of elevated FASN1 activity (Figure 3A) and insulin resistance. Interestingly, all of this occurs without genetically manipulating insulin signaling or any gene involved in glucose or lipid homeostasis. Simply elevating MG levels *in vivo* appears to induce both the insulin resistance and the metabolic defects observed in type 2 diabetic patients.

The current paradigm of T2D is that insulin resistance and hyperglycemia are root causes of the disease (Figure 4E, left). This leads to an elevation in MG levels, presumably due to elevated flux through glycolysis. Elevated MG can then mediate much of the tissue damage caused by the hyperglycemia. The data presented here raise the alternate hypothesis that elevated MG levels, due to either elevated MG production or impaired MG detoxification, could be a cause of T2D, leading to many of the phenotypes observed in patients (Figure 4E, right). We find here that elevated MG in an organism due to impaired detoxification leads to progressive development of obesity, hyperglycemia, and insulin resistance. This places MG not only downstream, but also upstream, of insulin resistance and hyperglycemia in terms of the chain of causality (Figure 4E, right), potentially generating a vicious cycle. This is in line with a recent report that pharmacological induction of Glo1 activity improves insulin sensitivity and glycemic control in patients (Xue et al., 2016), and that Glo1 has been linked as a top hit in epidemiological studies for coronary artery disease (Makinen et al., 2014) and hypertension (Wilson et al., 1991). MG is produced via multiple pathways, and multiple regulatory mechanisms could impinge on MG detoxification. This raises the possibility that alternate molecular mechanisms could account for elevated MG levels in patients in addition to hyperglycemia. Indeed, elevated MG has also been observed in patients that are obese, but not hyperglycemic, and this was attributed to MG production from the triosephosphate intermediates in the glyceroneogenic pathway required for triglyceride cycling (Masania et al., 2016). Thus, understanding the molecular mechanisms modulating MG production and detoxification may serve important avenues for future research in understanding the etiology of T2D.

The phenotypes displayed by $Glo1^{KO}$ animals appear not to be pleiotropic, but specific. They all relate to the regulation of central energy metabolism. Hence it is unlikely that MG is acting as a general, "toxic" metabolite. Indeed, animals with elevated levels of a toxic metabolite would be expected to have reduced longevity compared with control animals. Instead, $Glo1^{KO}$ animals have an extended lifespan. Interestingly, the accompanying paper by Ristow and colleagues (Ravichandran et al., 2018) finds an analogous lifespan extension in worms upon mildly elevated MG levels, suggesting this is an evolutionarily conserved response. We do not study here the molecular causes of the lifespan extension of the $Glo1^{KO}$ animals. Although one plausible explanation could be their reduced insulin signaling (Partridge et al., 2011), future work including genetic epistasis experiments will be required to understand this at the molecular level. In sum, just as hydrogen peroxide was at first thought to be an unavoidable toxic side product of respiration, and then found to play important roles in cell signaling, the data presented here suggest physiological levels of MG play a role in modulating organismal physiology.

Limitations of Study

One limitation of this study is that it was performed in *Drosophila*; hence, clinical implications can be drawn only once similar studies are conducted in mammalian systems. We have observed in many different contexts that metabolic regulation is highly conserved from flies to humans because it is evolutionarily ancient. Hence, it will be exciting to see the phenotypes of Glo1 knockout mice in the future. Another limitation is that metabolic flux analysis is difficult to perform *in vivo* in *Drosophila* because flies cannot be fed with the necessary time resolution. Hence, future studies will be needed to study in detail the effects of MG on cellular metabolic flux.

STAR★METHODS

Detailed methods are provided in the online version of this paper and include the following:

- KEY RESOURCES TABLE
- CONTACT FOR REAGENT AND RESOURCE SHARING
- EXPERIMENTAL MODEL AND SUBJECT DETAILS
  - Fly Stocks
  - Glo1 Knockout and Rescue Flies
  - Fly Growth/Culturing Conditions
  - Cell Culture
- METHOD DETAILS
  - Glyoxalase Activity Assay
  - Fatty Acid Synthase Activity Assay
  - AKR Activity Assay
  - MG Dehydrogenase Activity Assay

- Methylglyoxal Treatment of Drosophila Cells
- MG Treatment of Cell Lysates and FASN IP
- Mass Spec. Quantification of MG and MG-H1
- Trehalose Measurements
- Food Intake
- TAG and Glycogen Measurements
- Circulating Glucose Measurements
- Pupation Curves
- Determination of Larval and Adult Viability
- Antibody Production
- Purification of Inclusion Bodies
- MG-H1 ELISA
- Starvation Resistance
- H_2O_2 Feeding
- Lifespan
- Treatment of Cultured Cells with dsRNA
- Immunoprecipitation
- Western Blot Analysis
- dIlp2HF ELISA
- Respirometry Analysis
- Synthesis of Click-MG
- Biotin Labeling via clickMG or Control Ester

● QUANTIFICATION AND STATISTICAL ANALYSIS

SUPPLEMENTAL INFORMATION

Supplemental Information includes four figures and one table and can be found with this article online at https://doi.org/10.1016/j.cmet.2018.02.003.

ACKNOWLEDGMENTS

This work was supported by DFG grants TE 766/6-1, SFB1118, and SFB1036, and by the Helmholtz Future Topic "Aging and Metabolic Programming (AMPro)".

AUTHOR CONTRIBUTIONS

A.M., J.W., D.P., and T.F. performed experiments. A.M., J.W., D.P., T.F., A.K.M., P.N., and A.A.T. designed experiments, evaluated data, and wrote the manuscript.

DECLARATION OF INTERESTS

The authors declare no competing financial interests.

Received: October 24, 2016
Revised: July 27, 2017
Accepted: February 6, 2018
Published: March 15, 2018

REFERENCES

Adam, W., Bialas, J., and Hadjiarapoglou, L. (1991). Kurzmitteilung/short communication A convenient preparation of acetone solutions of dimethyldioxirane. Chem. Ber. *124*, 2377.

Ahmed, N., Babaei-Jadidi, R., Howell, S.K., Thornalley, P.J., and Beisswenger, P.J. (2005). Glycated and oxidized protein degradation products are indicators of fasting and postprandial hyperglycemia in diabetes. Diabetes Care *28*, 2465–2471.

Bellen, H.J., and Yamamoto, S. (2015). Morgan's legacy: fruit flies and the functional annotation of conserved genes. Cell *163*, 12–14.

Berlanga, J., Cibrian, D., Guillen, I., Freyre, F., Alba, J.S., Lopez-Saura, P., Merino, N., Aldama, A., Quintela, A.M., Triana, M.E., et al. (2005). Methylglyoxal administration induces diabetes-like microvascular changes and perturbs the healing process of cutaneous wounds. Clin. Sci. (Lond) *109*, 83–95.

Bierhaus, A., Fleming, T., Stoyanov, S., Leffler, A., Babes, A., Neacsu, C., Sauer, S.K., Eberhardt, M., Schnolzer, M., Lasitschka, F., et al. (2012). Methylglyoxal modification of Nav1.8 facilitates nociceptive neuron firing and causes hyperalgesia in diabetic neuropathy. Nat. Med. *18*, 926–933.

Brown, A., Reynolds, L.R., and Bruemmer, D. (2010). Intensive glycemic control and cardiovascular disease: an update. Nat. Rev. Cardiol. *7*, 369–375.

Chaudhuri, J., Bose, N., Gong, J., Hall, D., Rifkind, A., Bhaumik, D., Peiris, T.H., Chamoli, M., Le, C.H., Liu, J., et al. (2016). A Caenorhabditis elegans model elucidates a conserved role for TRPA1-Nrf signaling in reactive alpha-dicarbonyl detoxification. Curr. Biol. *26*, 3014–3025.

Currie, C.J., Peters, J.R., Tynan, A., Evans, M., Heine, R.J., Bracco, O.L., Zagar, T., and Poole, C.D. (2010). Survival as a function of HbA(1c) in people with type 2 diabetes: a retrospective cohort study. Lancet *375*, 481–489.

Garrido, D., Rubin, T., Poidevin, M., Maroni, B., Le Rouzic, A., Parvy, J.P., and Montagne, J. (2015). Fatty acid synthase cooperates with glyoxalase 1 to protect against sugar toxicity. PLoS Genet. *11*, e1004995.

Giacco, F., Du, X., D'Agati, V.D., Milne, R., Sui, G., Geoffrion, M., and Brownlee, M. (2014). Knockdown of glyoxalase 1 mimics diabetic nephropathy in nondiabetic mice. Diabetes *63*, 291–299.

Godfrey, L., Yamada-Fowler, N., Smith, J., Thornalley, P.J., and Rabbani, N. (2014). Arginine-directed glycation and decreased HDL plasma concentration and functionality. Nutr. Diabetes *4*, e134.

Golej, J., Hoeger, H., Radner, W., Unfried, G., and Lubec, G. (1998). Oral administration of methylglyoxal leads to kidney collagen accumulation in the mouse. Life Sci. *63*, 801–807.

Hahn, K., Miranda, M., Francis, V.A., Vendrell, J., Zorzano, A., and Teleman, A.A. (2010). PP2A regulatory subunit PP2A-B' counteracts S6K phosphorylation. Cell Metab. *11*, 438–444.

Han, T.S., and Lean, M.E. (2016). A clinical perspective of obesity, metabolic syndrome and cardiovascular disease. JRSM Cardiovasc. Dis. *5*, 2048004016633371.

Ismail-Beigi, F., Craven, T., Banerji, M.A., Basile, J., Calles, J., Cohen, R.M., Cuddihy, R., Cushman, W.C., Genuth, S., Grimm, R.H., Jr., et al. (2010). Effect of intensive treatment of hyperglycaemia on microvascular outcomes in type 2 diabetes: an analysis of the ACCORD randomised trial. Lancet *376*, 419–430.

Lenz, T., Fischer, J.J., and Dreger, M. (2011). Probing small molecule-protein interactions: a new perspective for functional proteomics. J. Proteomics *75*, 100–115.

Makinen, V.P., Civelek, M., Meng, Q., Zhang, B., Zhu, J., Levian, C., Huan, T., Segre, A.V., Ghosh, S., Vivar, J., et al. (2014). Integrative genomics reveals novel molecular pathways and gene networks for coronary artery disease. PLoS Genet. *10*, e1004502.

Masania, J., Malczewska-Malec, M., Razny, U., Goralska, J., Zdzienicka, A., Kiec-Wilk, B., Gruca, A., Stancel-Mozwillo, J., Dembinska-Kiec, A., Rabbani, N., et al. (2016). Dicarbonyl stress in clinical obesity. Glycoconj. J. *33*, 581–589.

Morgenstern, J., Fleming, T., Schumacher, D., Eckstein, V., Freichel, M., Herzig, S., and Nawroth, P. (2017). Loss of glyoxalase 1 induces compensatory mechanism to achieve dicarbonyl detoxification in mammalian schwann cells. J. Biol. Chem. *292*, 3224–3238.

Nepokroeff, C.M., Lakshmanan, M.R., and Porter, J.W. (1975). Fatty-acid synthase from rat liver. Methods Enzymol. *35*, 37–44.

Palmer, I., and Wingfield, P.T. (2004). Preparation and extraction of insoluble (inclusion-body) proteins from Escherichia coli. Curr. Protoc. Protein Sci. *Chapter 6*. Unit 6.3.

Park, S., Alfa, R.W., Topper, S.M., Kim, G.E., Kockel, L., and Kim, S.K. (2014). A genetic strategy to measure circulating Drosophila insulin reveals genes regulating insulin production and secretion. PLoS Genet. *10*, e1004555.

Partridge, L., Alic, N., Bjedov, I., and Piper, M.D. (2011). Ageing in Drosophila: the role of the insulin/Igf and TOR signalling network. Exp. Gerontol. *46*, 376–381.

Rabbani, N., and Thornalley, P.J. (2014). Measurement of methylglyoxal by stable isotopic dilution analysis LC-MS/MS with corroborative prediction in physiological samples. Nat. Protoc. *9*, 1969–1979.

Rabbani, N., and Thornalley, P.J. (2015). Dicarbonyl stress in cell and tissue dysfunction contributing to ageing and disease. Biochem. Biophys. Res. Commun. *458*, 221–226.

Ramasamy, R., Yan, S.F., and Schmidt, A.M. (2006). Methylglyoxal comes of AGE. Cell *124*, 258–260.

Ravichandran, M., Priebe, S., Grigolon, G., Ronzarov, L., Groth, M., Laube, B., Guthke, R., Platzer, M., Zarse, K., and Ristow, M. (2018). Impairing L-threonine catabolism promotes healthspan through proteotoxic methylglyoxal. Cell Metab. *27*. Published online March 15, 2018. https://doi.org/10.1016/j.cmet.2018.02.003.

Riboulet-Chavey, A., Pierron, A., Durand, I., Murdaca, J., Giudicelli, J., and Van Obberghen, E. (2006). Methylglyoxal impairs the insulin signaling pathways independently of the formation of intracellular reactive oxygen species. Diabetes *55*, 1289–1299.

Skriver, M.V., Borch-Johnsen, K., Lauritzen, T., and Sandbaek, A. (2010). HbA1c as predictor of all-cause mortality in individuals at high risk of diabetes with normal glucose tolerance, identified by screening: a follow-up study of the Anglo-Danish-Dutch Study of Intensive Treatment in People with Screen-Detected Diabetes in Primary Care (ADDITION), Denmark. Diabetologia *53*, 2328–2333.

Srivastava, S., Watowich, S.J., Petrash, J.M., Srivastava, S.K., and Bhatnagar, A. (1999). Structural and kinetic determinants of aldehyde reduction by aldose reductase. Biochemistry *38*, 42–54.

Sykiotis, G.P., and Bohmann, D. (2008). Keap1/Nrf2 signaling regulates oxidative stress tolerance and lifespan in Drosophila. Dev. Cell *14*, 76–85.

Thornalley, P.J. (1996). Pharmacology of methylglyoxal: formation, modification of proteins and nucleic acids, and enzymatic detoxification–a role in pathogenesis and antiproliferative chemotherapy. Gen. Pharmacol. *27*, 565–573.

Thornalley, P.J. (2008). Protein and nucleotide damage by glyoxal and methylglyoxal in physiological systems–role in ageing and disease. Drug Metabol. Drug Interact. *23*, 125–150.

Thornalley, P.J., Battah, S., Ahmed, N., Karachalias, N., Agalou, S., Babaei-Jadidi, R., and Dawnay, A. (2003). Quantitative screening of advanced glycation endproducts in cellular and extracellular proteins by tandem mass spectrometry. Biochem. J. *375*, 581–592.

Thornalley, P.J., and Rabbani, N. (2011). Glyoxalase in tumourigenesis and multidrug resistance. Semin. Cell Dev. Biol. *22*, 318–325.

Vander Jagt, D.L., and Hunsaker, L.A. (2003). Methylglyoxal metabolism and diabetic complications: roles of aldose reductase, glyoxalase-I, betaine aldehyde dehydrogenase and 2-oxoaldehyde dehydrogenase. Chem. Biol. Interact. *143-144*, 341–351.

Wilson, A.F., Elston, R.C., Tran, L.D., and Siervogel, R.M. (1991). Use of the robust sib-pair method to screen for single-locus, multiple-locus, and pleiotropic effects: application to traits related to hypertension. Am. J. Hum. Genet. *48*, 862–872.

Xue, M., Weickert, M.O., Qureshi, S., Kandala, N.B., Anwar, A., Waldron, M., Shafie, A., Messenger, D., Fowler, M., Jenkins, G., et al. (2016). Improved glycemic control and vascular function in overweight and obese subjects by glyoxalase 1 inducer formulation. Diabetes *65*, 2282–2294.

Yudkin, J.S., Richter, B., and Gale, E.A. (2010). Intensified glucose lowering in type 2 diabetes: time for a reappraisal. Diabetologia *53*, 2079–2085.

STAR★METHODS

KEY RESOURCES TABLE

REAGENT or RESOURCE	SOURCE	IDENTIFIER
Antibodies		
Anti MG-H1 guinea-pig polyclonal	This paper	N/A
Anti FASN1 guinea-pig polyclonal	This paper	N/A
Anti Glo1 rabbit polyclonal	Santa Cruz	sc-67351; RRID: AB_1124969
Anti-Tubulin mouse monoclonal	Hybridoma	Cat#AA4.3-s; RRID: AB_579793
Anti S6K guinea-pig polyclonal	(Hahn et al., 2010)	N/A
Anti pS6K (T398) rabbit polyclonal	Cell Signaling	9209S; RRID: AB_2269804
Anti AKT rabbit polyclonal	Cell Signaling	9272; RRID: AB_329827
Anti pAKT(S505) rabbit polyclonal	Cell Signaling	4054; RRID: AB_331414
anti-FLAG antibody	Sigma	F1804; RRID: AB_262044
Chemicals, Peptides, and Recombinant Proteins		
Complete protease inhibitor cocktail	Roche	Cat#15728900
PhosStop phosphatase inhibitor cocktail	Roche	Cat#04906837001
Lipoprotein lipase from Chromobacterium viscosum	Calbiochem	Cat#437707
Free Glycerol Reagent	Sigma	Cat#F6428
amyloglucosidase	Sigma	Cat#10115
Glucose reagent	Sigma	Cat#G3293
methylglyoxal	Sigma	Cat#M0252
Reduced L-Glutathione	Sigma	Cat#G6013
acetyl-CoA	Sigma	Cat#A2056
Malonyl-CoA	Sigma	Cat#M4263
NADPH	Applichem	Cat#A1395,0100
Gelatin	Sigma	Cat#G9382
TMB	Thermo Scientific	Cat#34028
Express Five Serum free medium	Gibco	Cat#10486-025
Flag beads	Sigma	Cat#A2220
Anti-HA-Peroxidase High Affinity (3F10)	Roche	Cat#12013819001
Streptavidin-HRP	Invitrogen	Cat#T20932
Experimental Models: Cell Lines		
D. melanogaster: Cell line S2	Laboratory of Michael Boutros	N/A
Experimental Models: Organisms/Strains		
D. melanogaster w^{1118}	Bloomington Drosophila Stock Center	Stock 3605
D. melanogaster w^{1118};Glo1[KO];+	This paper	N/A
D. melanogaster w^{1118};+;UAS-Glo1	This paper	N/A
D. melanogaster w^{1118};+; *daugtherless*Gal4/TM3	Bloomington Drosophila Stock Center	Stock 55851
D. melanogaster yw;+;Ilp2-gd2HF(attP2)	Pierre Leopold	N/A
Oligonucleotides		
Cloning and gene expression knockdown oligonucleotides	This paper	Table S1
Recombinant DNA		
pMT-FASN1-Flag	This paper	N/A
pETM-N-fragment-FASN1 for antibody production	This paper	N/A

CONTACT FOR REAGENT AND RESOURCE SHARING

Further information and requests for resources and reagents should be directed to and will be fulfilled by the Lead Contact, Aurelio Teleman (a.teleman@dkfz.de).

EXPERIMENTAL MODEL AND SUBJECT DETAILS

Fly Stocks

w^{1118} and daughterless-GAL4 flies are from Bloomington Drosophila Stock Center. Glo1[KO] and UAS-Glo1 flies were generated as described below. Flies carrying an HF-tagged dILP2 genomic locus were described in Park et al. (2014).

Glo1 Knockout and Rescue Flies

Glo1[KO] flies were generated by imprecise excision of a P element inserted in the 5'UTR region having the FlyBase ID Dmel\P{GT1}Glo1^{BG02656}, which yielded a 1136nt deletion covering the translation start site and the first 3 exons of Glo1. The genetic background of Glo1[KO] flies was cleaned by 4 generations of backcrossing to an isogenic w^{1118} stock, which is used as the control stock in all experiments described here. The rescue construct used to make UAS-Glo1 animals was generated by cloning the Glo1 CDNA sequence into pUAST.

Fly Growth/Culturing Conditions

For all growth and metabolic measurements, flies were grown under controlled conditions: Flies were allowed to lay eggs on apple plates for 12 hours. First instar larvae hatching within a 4 or 6 hour window were picked and seeded at a density of 60 animals per vial. Adult flies of all genotypes eclosing within a 24-hour time-window were mated for 48 hours, then separated by gender, and finally aged an equal number of days. All metabolic analyses shown in the figures are done on females, as indicated in the figure legends. Males have similar metabolic phenotypes as females, albeit more mild than females, as is usually the case in Drosophila (likely due to the high metabolic requirements of females due to egg laying).

Flies were grown and maintained on food consisting of the following ingredients for 30 liters of food: 480g agar, 660g sugar syrup, 2400g malt, 2400g corn meal, 300g soymeal, 540g yeast, 72g nipagin, 187mL propionic acid and 18.7 mL phosphoric acid. For TAG, glycogen, circulating sugar, lifespan, feeding and FAS activity assays, the food was diluted to 20% in 1% agarose/1xPBS. Mated females flies were transferred to this 20% food and aged for the indicated amount of time prior to metabolic analyses.

Cell Culture

Drosophila embryonic Schneider 2 (S2) cells were maintained at 25°C in Express Five Serum free medium (SFM Gibco #10486-025) supplemented with 5% L-Glutamine and 1% Penicillin/Streptomycin in culture flasks (75cm^2).

METHOD DETAILS

Glyoxalase Activity Assay

10 growth-controlled flies (see "Fly Growth/Culturing Conditions" above) were homogenized in 1 mL homogenization buffer (10mM sodium phosphate buffer pH 7.0, 0.02% Triton X-100) and subjected to sonication using a Branson sonifier for 15 sec with 30% power, followed by centrifugation at 14,000 rpm, 30 min at 4°C. The substrate mix was prepared as follows: 50 mM sodium phosphate buffer pH 6.6, 10 mM Methylglyoxal (Sigma M0252), 10 mM reduced L-Glutathione (Sigma G6013) and was incubated for 10 min at 37°C. 10 μL of cleared fly lysate were added to 100 μL substrate mix. The changes in absorption at 235 nm were recorded for a total duration of 15 min using the SPECTROstar Omega plate reader (BMG LABTECH).

Fatty Acid Synthase Activity Assay

Flies were crushed in homogenization buffer (10mM potassium phosphate buffer pH7.4, 1mM EDTA, 1mM DTT). Precipitation of the lysate was performed with ammonium sulfate to remove metabolites and other small molecules which could generate high background. A saturated ammonium sulfate solution (4.1 M at room temperature) was prepared and the twofold volume of the lysate was added. After incubation on ice for 20 min the suspension was centrifuged at 14,000 rpm for 5 min at 4°C. The supernatant was carefully discarded and the pellet resuspended in the original volume of homogenization buffer.

For performing the assay in cell lysates, 2 x 10^6 cells were prepared by spinning them down at 1500 rpm for 3 min and discarding the medium. The cells were suspended in ice-cold homogenization buffer and subjected to sonication (15 sec, 20% power) to facilitate cell lysis and release of cytosolic enzymes.

The assay reaction mix (modified from Nepokroeff et al., 1975) contains 20 mM Tris pH 8.0, 0.033 mM acetyl-CoA, 0.1 mM malonyl-CoA and 0.2 mM NADPH. Tris buffer, NADPH and 10 μL of fly lysate were mixed in 96-well-UV-plates and incubated for 10 min. The fatty acid synthase substrates malonyl-CoA and acetyl-CoA were mixed and added to the solution directly before starting the measurement. The changes in absorption at 340 nm were recorded in 2 min intervals for a total duration of 1 hour using the

SPECTROstar Omega plate reader (BMG LABTECH). One unit of enzymatic activity corresponds to the amount of enzyme that is needed to synthesize 1 nmol of palmitic acid (which is equivalent to oxidation of 14 nmol NADPH) per minute and is calculated with the following formula:

$$Activity\left[\frac{U}{\mu L}\right] = \frac{\Delta Abs_{340nm} * V_{total}}{\Delta t * \varepsilon_{340nm}\ (=6.22) * 14 * V_{sample}}\ .$$

AKR Activity Assay

The assay for AKR activity was adapted from Morgenstern et al. (2017) and Srivastava et al. (1999). 10 larvae were homogenized in 1 mL homogenization buffer (10mM sodium phosphate buffer pH 7.2, 0.02% Triton X-100) and subjected to sonication using a Branson sonifier for 10 sec with 30% power, followed by centrifugation at 14,000 rpm, 30 min at 4°C. The substrate mix was prepared as follows: 100 mM sodium phosphate buffer pH 7.2, 0.1 mM NADPH and varying amounts of MG (0.125 to 2 mM). 10 μL of cleared larval lysate were added to 190 μL substrate mix. The oxidation of NADPH was monitored at RT by measuring the absorption at 340nm for a total duration of 20 min using the SPECTROstar Omega plate reader (BMG LABTECH).

MG Dehydrogenase Activity Assay

Although we could detect no MG dehydrogenase activity above background in fly lysates, the following assay adapted from Morgenstern et al. (2017) and Vander Jagt and Hunsaker (2003) was used. 10 larvae were homogenized in 1 mL homogenization buffer (10mM sodium phosphate buffer pH 7.2, 0.02% Triton X-100) and subjected to sonication using a Branson sonifier for 10 sec with 30% power, followed by centrifugation at 14,000 rpm, 30 min at 4°C. The substrate mix was prepared as follows: 75 mM Tris-HCl (pH 9.5) containing 10 mM DL-2-amino-1-propanol, 0.5 mM NAD or NADP and varying amounts of MG (0.125 to 2 mM). 10 μL of cleared larval lysate were added to 190 μL substrate mix. The reduction of NAD or NADP was monitored at RT by measuring the absorption at 340nm for a total duration of 20 min using the SPECTROstar Omega plate reader (BMG LABTECH).

Methylglyoxal Treatment of Drosophila Cells

Drosophila S2 cells were seeded into a 12-well plate (10^6 cells/well). Methylglyoxal was diluted in SFM and added to the cell to the indicated concentrations and amount of time. For Western blot analysis the cells were lysed into Laemmli buffer. For intracellular methylglyoxal determination the cells were collected by centrifugation and snap frozen in liquid nitrogen.

MG Treatment of Cell Lysates and FASN IP

Drosophila S2 cells were lysed in 50mM Tris pH7.5, 1% Triton X-100, 150mM NaCl, 2x Complete protease inhibitor cocktail without EDTA, clarified by centrifugation, then incubated for 6 hours at RT with various concentrations of MG as indicated in the figures. FASN1-FLAG was cloned in 3 pieces using oligos OAM277, OAM280, OAM283, OAM284, OAM285 and OAM286 (sequences in Table S1) into pMT-Flag C terminal (plasmid pAT1166). For immunoprecipitation of FASN1-FLAG, the lysates were treated with or without 0.5 mM MG for 4 hours at RT, followed by an additional 2 hours incubation with anti-FLAG beads. The beads were then washed with IP buffer 4 times, then boiled in Laemmli buffer containing DTT. The proteins were separated by SDS-PAGE and the corresponding FASN1-FLAG band was cut out, eluted from the gel in 50mM Tris pH7.5, 150 mM NaCl, 0.1mM EDTA and analyzed for MG-H1 levels as detailed below.

Mass Spec. Quantification of MG and MG-H1

Methylglyoxal levels in cells was determined by liquid chromatography with tandem mass spectrometric detection (LC-MS/MS), as described previously (Rabbani and Thornalley, 2014).

Protein-bound MG-H1 was determined by isotope-dilution, liquid chromatography-tandem mass spectrometry after exhaustive enzymatic hydrolysis, as described in Thornalley et al. (2003) and normalized to total arginine content.

Trehalose Measurements

6 flies were homogenized in 0.5 mL 70% ethanol. The samples were centrifuged 5 minutes at 14000 rpm at RT, followed by vacuum centrifugation at 45°C for ca. 45 minutes until the samples were dried. Lyophilized material was resuspended in 200 μL of 2% NaOH and incubated at 100°C for 10 minutes. 40 μL of the prepared sample was mixed with 1 mL of Anthrone reagent 0.2 %(w/v) in 72% sulphuric acid, incubated at 90°C for 20 minutes, and cooled down to RT. Absorbance was measured at 620nm.

Food Intake

Flies were placed on food supplemented with 1% (w/w) Acid blue for 2 hours at RT while keeping the tube horizontally. 10 flies per replicate were homogenized in 0.5mL of 0.05% Tween in PBS. Lysates were cleared by spinning samples at 14,000 rpm for 20 min, followed by separation of organic and aqueous phase by adding half the volume of chloroform and centrifuging at 14,000 rpm for

15 min. The aqueous phase was transferred into a 96-well plate and absorption at 625 nm was measured with the SPECTROstar Omega plate reader (BMG LABTECH).

TAG and Glycogen Measurements

TAG content and glycogen content of flies were measured simultaneously using a combined assay. Triplicates of 8 female flies per sample were homogenized in 500 μl of PBST (0.05% (v/v) Tween 20 in PBS) using a table-top drill with a plastic pestle. 200 μl of lysate was incubated at 70°C for 5 min, chilled on ice, and incubated with 1μL of 25KU/mL Lipoprotein lipase from Chromobacterium viscosum (Calbiochem, cat. 437707) at 37°C overnight. Cellular debris were removed by centrifugation at 14000rpm for 3 min. TAG content was determined by mixing 15 μl of the supernatant with 150 μl Free Glycerol Reagent (Sigma F6428), incubated at 37°C for 6 min and absorbance was measured at 540nm. Data were normalized to total protein measured by Bradford assay at 595nm. For determining the glycogen content 30 μl of the supernatant (after LPL treatment) was treated with 14Units of amyloglucosidase (Sigma 10115) at 50°C for 1hour. 15 μl of the treated mix was combined with 150 μl of glucose reagent (Sigma G3293), incubated at 37°C for 30 min and absorbance was measured at 340nm. These data were also normalized to total protein.

Circulating Glucose Measurements

For larval hemolymph, hemolymph was collected from 8 third instar larvae into TBS pH6.6 (137mM NaCl, 2.7mM KCl, 5mM Tris pH6.6), followed by heat-inactivation at 70°C for 5 min.

For adult hemolymph, adult flies were anaesthetized with carbon dioxide in a humid environment and pinched through the thorax with a micro dissecting needle. About 40 flies were then transferred into a small collection tube with a perforated bottom, which was afterwards placed into 1.5 mL collection tube and centrifuged at 5,000 rpm for 5 min at 0°C.

In both cases, free glucose was then measured using a colorimetric kit from Sigma (G3293)

Pupation Curves

Fifty first-instar larvae were seeded per vial, in triplicate for each genotype, and grown under controlled conditions, in standard food at 25°C as described above. The number of pupated animals was counted over time, and is represented as a percentage of total pupated animals.

Determination of Larval and Adult Viability

For larval viability, 100 embryos were collected, in triplicates for each genotype. The number of hatched larvae was counted over time, and is represented as percentage of total collected embryos, normalized to control.

For adult viability, 50 larvae were collected, in tetraplicates for each genotype. The number of hatched adults was counted over time, and is represented as percentage of total collected larvae, normalized to control.

Antibody Production

To generate anti-Drosophila FASN1 antibody, a His-tagged N-terminal fragment of the FASN1 protein was produced by amplifying the coding sequence corresponding to amino acids 1-216 into the pETM11 plasmid, and expressing it in BL21 E coli. Because the protein was highly insoluble, inclusion bodies containing the protein were purified (see "Purification of inclusion bodies" below) and then used to immunize guinea pigs.

To generate anti MG-H1 antibody, synthetic MG-H1 was conjugated to KLH by glutaraldehyde cross-linker and then used to immunize guinea pigs.

Purification of Inclusion Bodies

The following steps were performed based on the protocol published by Palmer and Wingfield (2004): DTT, urea and Triton X-100 were added to the wash buffer right before use and additionally a urea- and Triton-free batch was prepared. The pellet was suspended in 1 mL wash buffer (+urea/Triton) by vigorous pipetting and vortexing prior to centrifuging at 22,000g for 30 min at 4°C. The residual supernatant was discarded and the described steps were repeated 3 times and for the last repetition washing buffer without urea and Triton was used.

MG-H1 ELISA

ELISAs with anti-MG-H1 antibody were performed by binding 50μL of 1 μM antigen in ammonium bicarbonate 100 mM pH9.6 into a 96-well plate. The plate was incubated at 37°C for 75 minutes. The content was then washed 3 times with PBS. Wells were then blocked with 0.5% (w/v) gelatin (SIGMA G9382) in PBS and incubated at 37°C for 75 minutes. The wells were washed 3 times with PBS, followed by incubation over night at 4°C with anti MG-H1 antibody in PBS in serial dilutions starting at 1:500. The wells were then washed 3 times with Tween 0.05% in PBS, followed by incubation with secondary antibody anti guinea-pig IgG diluted 1:5000 37°C for 75 min. Developing reagent TMB (Thermo Scientific 34028) was added and absorbance recorded on a microplate reader.

Starvation Resistance

1 week old adult female flies, grown under controlled conditions as described above, were transferred from normal food to 1% agarose/PBS and dead animals were counted over time.

H_2O_2 Feeding

1 week old female flies were kept horizontally at 25 degrees in vials containing either normal food supplemented with indicated concentrations of H_2O_2 (w/v) or 5% glucose/ 1% agarose/ PBS supplemented with or without 3% H_2O_2.

Lifespan

For lifespan measurement, back-crossed animals (see above) were raised in controlled growth conditions (50 larvae per vial) as described above, and co-aged adults were then kept at 25 degrees in horizontally-positioned vials. Animals were transferred into fresh vials every 3 days to prevent molding.

Treatment of Cultured Cells with dsRNA

dsRNA was generated using T7 *in vitro* transcription. Gene knockdowns were performed by treating S2 cells with 12ug/ml dsRNA for 5 days. Oligos for generating dsRNA are listed in Table S1.

Immunoprecipitation

Flies or cells were lysed in IP lysis buffer (50mM Tris pH7.5, 1% Triton X-100, 150mM NaCl, 1.5x Complete protease inhibitor cocktail without EDTA, 2x PhosStop phosphate inhibitor cocktail, 4mM Na vanadate, 100mM Na fluoride, 11mg/mL beta-glycerophosphate), clarified by centrifugation, incubated with indicated antibody for 3 hours at 4°C, followed by incubation with protein A beads for 30 minutes at 4°C, then washed with IP buffer 4 times. The beads were boiled in reducing Laemmli buffer and analyzed by Western blotting.

Western Blot Analysis

For SDS-PAGE and immunoblotting experiments, flies were lysed in 1xLaemmli lysis buffer (100 mM NaF, 4 mM Na-vanadate, 0.02 gr/ml beta-glycerophosphate, 2× PhosSTOP phosphatase inhibitors and 2× Complete protease inhibitors). The antibodies used for detection were the following: anti-Glo1 1:1000 (Santa Cruz sc-67351 lot no #G0208), anti-pS6K T398 1:2000 (Cell Signaling 9209S), anti-dS6K 1:2000 (Hahn et al., 2010), anti-AKT (Cell Signaling 9272), anti-pAKT S505 (Cell Signaling 4054), anti-dFASN1 1:1000 (self-made, see above), anti-MG-H1 1:500 (self-made, see above).

dIlp2HF ELISA

The HF-tagged dILP2 genomic locus (Park et al., 2014) was crossed into the control or the $Glo1^{KO}$ genetic background. Coated plates (Greiner 655061) containing 100 μl of 2.5 μg/ml anti-FLAG antibody (Sigma-Aldrich F1804) diluted in 0.2M sodium carbonate/bicarbonate buffer, pH 9.4, were sealed with tape and incubated overnight at 4°C. The plates were then washed twice with 250 μL 0.2% Tween 20 in 1xPBS and blocked with 200 μl of 2%BSA/PBS overnight at 4°C.

Two μL of hemolymph were collected from seven L3 larvae or 30 adult flies (tightly growth controlled) and transferred into 1.5mL tubes containing 55 μl of PBS on ice. These tubes were then centrifuged at 1,000g for 1 min, and 50 μl of supernatant was transferred to PCR tubes. Anti-HA-Peroxidase, High Affinity (3F10) (Roche 12013819001; 25 μg/mL) was prepared in PBS with 2% Tween 20 at a 1:350 dilution. 5 μL of the diluted anti-HA-Peroxidase was dispensed into the PCR tubes containing the hemolymph, vortexed, and centrifuged briefly. The blocked ELISA plates were washed three times with wash buffer (0.2% Tween 20 in 1xPBS). The samples were then transferred into the ELISA plates and incubated overnight at 4°C. The plates were then washed six times with wash buffer. 100 μL of 1-Step Ultra TMB - ELISA Substrate (Thermo Scientific 34028) were added per well, and incubated 25 min at RT. The reaction was stopped by adding 100 μL 2M sulfuric acid and the absorbance at 450nm was measured immediately.

Respirometry Analysis

Females were grown under controlled conditions as described above in the section "Fly Growth/Culturing Conditions". At 1 week of age, the flies were transferred to glass respirometry vials of a standard Sable Systems stop-flow insect respirometer, at 10 flies per vial. These tubes were connected to a RM-8 multiplexer, which feeds into a CA-10 Carbon Dioxide Analyzer, which then feeds into a FC-10 Oxygen Analyzer. VO_2 and VCO_2 were analyzed for 5 minutes per tube. Multiple successive runs were performed to allow for recovery from the initial CO_2 anesthesia during transfer. The first two runs were disregarded. Measured data was transferred to a computer via UI-3 Universal Interface. Recording and analysis was performed with Expedata-P Data Analysis Software. Fresh air is pumped into the system via a SS-4 Gas Analyzer Subsampler. All components of the respirometry setup were provided by Sable Systems Europe, except for the Side-Trak 840 (Sierra Instruments) component connected to the MFC2 mass flow valve controller unit.

Synthesis of Click-MG

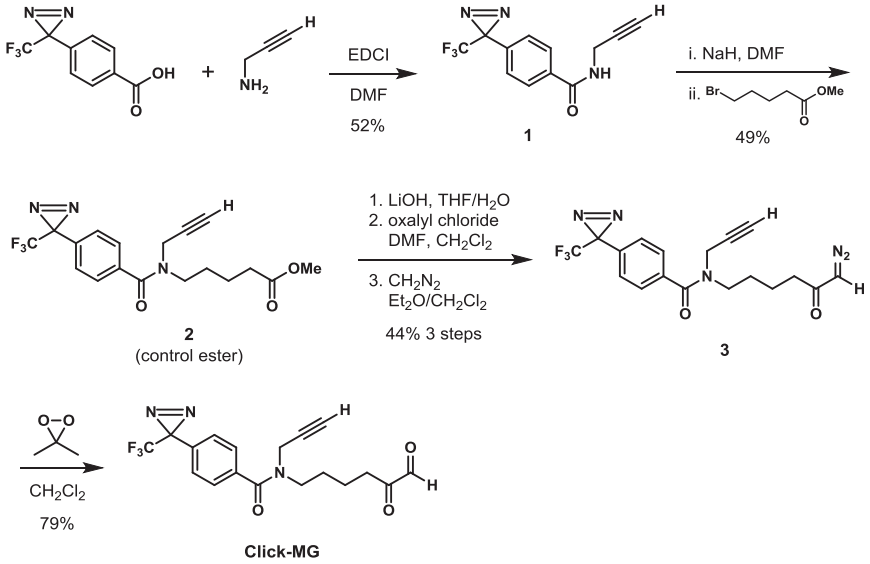

General Synthetic Chemistry

Analytical thin layer chromatography (TLC) was carried out on Merck silica gel 60 F_{254} TLC plates. TLC visualization was accomplished using 254 nm UV light and staining in an I_2 chamber. Flash column chromatography was performed using SiliCycle SiliaFlash E60 silica gel (15-40 μm particle size). Automated flash chromatography was performed on a Teledyne ISCO Combiflash R_f using prepacked SiO_2 columns, with preloading of the crude sample on coarse Silica Gel 60 (Roth). NMR spectra were recorded on a Bruker Ultrashield 400 in using the residual solvent peak as internal reference ($CHCl_3$ @ 7.26 ppm ^{1}H NMR; 77.16 ppm ^{13}C NMR, CD_3SCD_2H @ 2.50 ppm ^{1}H NMR; 39.52 ppm ^{13}C NMR, CD_2HOD 3.31 ppm ^{1}H NMR; 49.00 ppm ^{13}C NMR).

N-(prop-2-yn-1-yl)-4-(3-(trifluoromethyl)-3H-diazirin-3-yl)benzamide (1)

To a solution of 4-(3-(trifluoromethyl)-3H-diazirin-3-yl)benzoic acid (1.191 g, 5.17 mmol) in DMF (10 mL) was added EDCI (1-ethyl-3-(3-dimethylaminopropyl)carbodiimide hydrochloride) (1.119 g, 5.84 mmol) followed by propargyl amine (315 mg, 5.72 mmol) at room temperature. After 18 h, the reaction was diluted with H_2O (150 mL), and the resulting white precipitate was filtered, washed with H_2O (3 x 25 mL), and dried under high vacuum to give 716 mg (52%) of **1** as a white solid.

R_f: 0.54 (40% EtOAc in hexanes)
^{1}H-NMR (400 MHz, $CDCl_3$): δ 7.81 (d, *J* = 8.5 Hz, 2 H), 7.26 (d, *J* = 8.5 Hz, 2 H), 6.31 (bs, 1 H), 4.25 (dd, *J* = 5.2, 2.6 Hz, 2 H), 2.3 (t, *J* = 2.6 Hz, 1 H) ppm.

Methyl 5-(N-(prop-2-yn-1-yl)-4-(3-(trifluoromethyl)-3H-diazirin-3-yl)benzamido)pentanoate (2)

To a solution of amide **1** (317 mg, 1.19 mmol) in anhydrous DMF (10 mL) was added NaH (58 mg, 1.45 mmol, 60% in oil) at room temperature under argon. The initially yellow-orange solution became blue, then dark greenish brown with bubbling. After 1.5 h, methyl bromovalerate (0.19 mL, 1.33 mmol) was added. The reaction did not proceed to completion, but was quenched after 18 h with H_2O (100 mL) and diluted with EtOAc (25 mL). The two layers were separated and the aqueous layer was extracted with EtOAc (2 x 25 mL). The combined organics were washed with H_2O (10 mL) and brine (10 mL), then dried ($MgSO_4$), filtered, and concentrated in vacuo. Note: the product is more polar by TLC than the starting material. A less polar side product is also produced but was never characterized. The product was purified by automated column chromatography (20–40% gradient of EtOAc in hexanes) to give 225 mg (49%) of **2** as a yellow oil.

R_f: 0.43 (40% EtOAc in hexanes)
^{1}H-NMR (400 MHz, CD_3OD) ~1.1:1.0 mixture of rotamers: δ 7.60 and 7.51 (bd, 2 H), 7.37 (d, *J* = 8.1 Hz, 2 H), 4.36 and 4.01 (s, 2 H), 3.66 (s, 3 H), 3.49, 3.64, and 3.36 (bs, 2 H), 2.85 and 2.73 (bs, 1 H), 2.42 and 2.20 (bs, 2 H), 1.82–1.60 and 1.50–1.37 (m, 4 H) ppm.

N-(6-diazo-5-oxohexyl)-N-(prop-2-yn-1-yl)-4-(3-(trifluoromethyl)-3H-diazirin-3-yl)benzamide (3)

To a solution of ester **2** (280 mg, 0.73 mmol) in THF (20 mL) was added a solution of LiOH (74 mg, 3.1 mmol) in H_2O (5 mL) at room temperature. After 18 h the reaction was quenched with a concentrated aqueous solution of NH_4Cl (50 mL) and was diluted with EtOAc (20 mL). The two layers were separated and the aqueous layer was extracted with EtOAc (2 x 20 mL). The combined organics were dried ($MgSO_4$), filtered, and concentrated in vacuo to give the corresponding carboxylic acid.

To a solution of this acid in CH_2Cl_2 (10 mL) was added oxalyl chloride (0.07 mL, 0.82 mmol) followed by DMF (1 drop). After 1 h, bubbling had ceased and the reaction was deemed complete by TLC (monitored by quench of a small sample into a dilute solution of DMAP in MeOH to convert the acid chloride into the corresponding methyl ester). The reaction was concentrated in vacuo. The resulting residue was redissolved in CH_2Cl_2 and concentrated twice before putting the crude acid chloride under high vacuum for 1 h. For the following reaction it was necessary to freshly prepare diazomethane with an Aldrich Mini Daizald Apparatus. This was accomplished by adding a solution of DIAZALD (260 mg, 1.21 mmol) in Et_2O (15 mL) dropwise via addition funnel into a solution of KOH in H_2O/EtOH (1 mL:4 mL) which was heated in a 65 °C oil bath. The resulting yellow ethereal distillate of diazomethane was condensed with a −78 °C cooled cold finger into a solution of the crude acid chloride in CH_2Cl_2 (10 mL) cooled to 0 °C. After the distillation was complete, a few drops of acetic acid were added to the reaction mixture. The reaction mixture was concentrated and purified by automated column chromatography (30 to 80% gradient of EtOAc in hexanes) to give 126 mg (44% over 3 steps) of **3** as a yellow oil.

R_f: 0.24 (50% EtOAc in hexanes)
^{1}H-NMR (400 MHz, $CDCl_3$) mixture of rotamers: δ 7.54 and 7.45 (bs, 2 H), 7.25 (d, *J* = 8.2 Hz, 2 H), 5.28 and 5.17 (bs, 1 H), 4.36 and 3.93 (bs, 2 H), 3.62 and 3.36 (bs, 2 H), 2.50–2.15 (m, 3 H), 1.80–1.45 (m, 4 H) ppm.
LC-MS (ESI) (*m/z*): $[M+Na]^+$ = 414.1; $[M–N_2+H]^+$ = 364.1.

N-(5,6-dioxohexyl)-N-(prop-2-yn-1-yl)-4-(3-(trifluoromethyl)-3H-diazirin-3-yl)benzamide (Click MG)

A solution of dimethyldioxirane (DMDO) was prepared according to the method of Adam (Adam et al., 1991): to a suspension of $NaHCO_3$ (29 g) in H_2O (127 mL) and acetone (96 mL) cooled in an ice bath, was added oxone (60 g) in five equal portions every three minutes for 12 minutes while vigorously stirring with an overhead stirrer. Three minutes after the last oxone addition, vacuum (120 mbar) was applied, the ice bath was removed from the reaction vessel, and the resulting distillate was collected in a −78 °C cooled round bottom flask. After ~75 mL of distillate had been collected, the distillate was dried over solid K_2CO_3 (10 g), and filtered through paper into a dry flask containing activated 4 Å molecular sieves. Iodometric titration gave a DMDO concentration in acetone of 0.099 M. To a solution of diazoketone **3** (59 mg, 0.15 mmol) in CH_2Cl_2 (2.0 mL) was added DMDO (1.67 mL, 0.165 mmol, 0.099 M in acetone) dropwise at room temperature. Immediate evolution of N_2 gas was observed. After 10 min, the reaction was deemed complete by TLC and the mixture was concentrated in vacuo. The product was purified by automated column chromatography (1% to 4% gradient of MeOH in CH_2Cl_2) to give 45 mg (79%) of Click MG as a colorless oil.

R_f: 0.11 (50% EtOAc in hexanes)
^{1}H-NMR (400 MHz, $CDCl_3$) mixture of rotamers: δ 7.54 and 7.45 (bs, 2 H), 7.25 (d, *J* = 8.2 Hz, 2 H), 4.78 and 4.35 (bs, 2 H), 4.06 and 3.94 (bs, 2 H), 3.70–3.30 (m, 3 H), 2.90–2.20 (m, 3 H), 1.80–1.40 (m, 4 H) ppm.
LC-MS (ESI) (*m/z*): $[M+H]^+$ = 380.1.

Biotin Labeling via clickMG or Control Ester

S2 cells in SFM were seeded in a 6 well plate at 12 million cells per well and allowed to adhere for 1 hour. After that, medium was replaced with 1 mL SFM containing 10 μM Click-MG or 10μM Click-control (Figure 3F) and allowed to incubate for 1 hour at 25 °C in the dark. Cells were then exposed to 5 minutes of UV irradiation at 365 nm by a 36W UV Lamp. The medium was then removed and 1 mL of lysis buffer (PBS with 1% Triton-X) was pipetted into each well. Lysis was performed by pipetting up and down repeatedly and then transferring the lysate to a 1.5 mL Eppendorf tube to incubate on ice for 10 minutes. Unlysed cells were pelleted by centrifuging at 4000 rpm for 2 minutes. Of the supernatant 50 μL were transferred to an Eppendorf tube containing 10 μL 18 megaOhm water and 100 μl Click-iT reaction buffer (Click-iT Protein Reaction Buffer Kit, Thermo Fisher #C10276) with 40 μM biotin azide (Thermo Fisher, #B10184). After vortexing 10 μL of CuSO4 were added, then after vortexing again 10 μL of Click-iT reaction buffer additive 1 solution. After vortexing and waiting for 3 minutes 20 μL of Click-iT reaction buffer additive 2 solution were added. The Eppendorf tubes were vortexed and set to rotate end-over-end for 20 minutes. After that, a methanol chloroform pelleting was performed with two methanol washing steps of the pellet and a 30 minute air drying step at the end. The protein pellet was resuspended in 50 μL 1% SDS, 30 mM Tris pH8, Roche protease inhibitor cocktail. The resuspension was diluted by adding 450 μL of 50 mM Tris pH 7.5, 150 mM NaCl, Roche protease inhibitor cocktail. Biotinylated proteins were pulled down with streptavidin coupled beads (Life Technologies 65001 Dynabeads MyOneStreptavidin C1) overnight by end-over-end rotation at 4°C. The beads were washed 2 times with wash buffer 1 (2% SDS in ddH2O), wash buffer 2 (0.1% deoxycholate, 1% Triton X-100, 500 mM NaCl, 1 mM EDTA, 50 mM Hepes, pH 7.5), wash buffer 3 (250 mM LiCl, 0.5 M NP-40, 0.5% deoxycholate, 1 mM EDTA, 10 mM Tris pH 8.1) and wash buffer 4 (50 mM Tris pH 7.4, 50 mM NaCl). The proteins were eluted off of the beads with 1mM biotin containing 2X Laemmli buffer for 15 minutes at room temperature and then 15 minutes at 95°C. Samples were then run in a SDS-PAGE electrophoresis, blotted and stained with anti-FASN1 or Streptavidin-HRP (Invitrogen, #T20932).

QUANTIFICATION AND STATISTICAL ANALYSIS

Statistical significance was tested using the student t-test, except for the survival curves shown in Figures 4B and 4D where significance was tested on entire distributions using a logrank significance test. Statistical tests were performed either with GraphPad Prism (for logrank test) or Microsoft Excel (for t-tests). P-scores greater than 0.05 were considered as not significant. All statistical tests and n values are indicated in the figure legends. T-test results are indicated consistently in all figures as *ttest<0.05, **ttest<0.01, ***ttest<0.001 and "n.s." for not significant ($p>0.05$).